Measurement of the occupation lengths of channeled 17-MeV electrons and 54-MeV electrons and positrons in silicon by means of channeling radiation

J. O. Kephart
Xerox Palo Alto Research Center, Palo Alto, California 94304

R. H. Pantell
Department of Electrical Engineering, Stanford University, Stanford, California 94305

B. L. Berman
Department of Physics, The George Washington University, Washington, D.C. 20052

S. Datz
Physics Division, Oak Ridge National Laboratory, Oak Ridge, Tennessee 37831

H. Park
AT&T Bell Laboratories, Allentown, Pennsylvania 18103

R. K. Klein
Advanced Micro Devices, Inc., Sunnyvale, California 94088
(Received 16 March 1989)

The occupation length of channeled 17-MeV electrons and 54-MeV electrons and positrons in silicon has been determined by measuring the intensity of the emitted channeling radiation. For 17-MeV electrons the measured $1/e$ occupation lengths are approximately 16 μm for the (100) plane and 20 μm for the (110) plane. For 54-MeV electrons the occupation lengths are 24 μm for the (100) plane and 36 μm for the (110) plane. For 54-MeV positrons the occupation lengths are 40, 60, and 42 μm for the (100), (110), and (111) planes, respectively. In all cases, the bound-state populations remain equal relative to one another throughout the thickness of the crystal. Multiple scattering appears to modify positron channeling radiation spectra slightly, but multiple scattering has no perceptible influence upon electron channeling radiation spectra.

I. INTRODUCTION

When a beam of charged particles is incident upon a target, it ordinarily scatters incoherently from the individual atoms which comprise the target. However, when the beam is directed into a crystal along a direction of high symmetry (a plane or an axis), the particles scatter coherently from the crystalline potential in such a way that they are guided along that plane or axis—a phenomenon known as "channeling." The transverse motion of a channeled particle is usually thought of as being governed by an effective "continuum potential,"[1] which is obtained by an appropriate spatial and temporal average of the true crystalline potential. The longitudinal motion is essentially free. If the transverse momentum of the particle is sufficiently small, it will be bound by the continuum potential, and the particle will undulate as it moves down the channel.

A number of interesting phenomena are associated with channeling, including the anomalously low backscattering of channeled positive ions[2] and the deflection of charged particle beams by bent crystals.[3,4] One interesting property of very light channeled particles such as electrons and positrons, which we have studied in our experiments, is their spontaneously emitted radiation spectrum. The undulatory motion of the charged particles gives rise to "channeling radiation" (CR), which can be considerably more intense than the background of bremsstrahlung radiation.[5,6]

Due to a variety of scattering processes, a channeled particle will eventually be scattered out of the channel, or "dechanneled." The length scale over which dechanneling occurs is not merely of theoretical interest; it is of great practical importance as well. For example, if particles remain channeled through an appreciable length, the spontaneous CR intensity could rival or surpass that of the most intense synchrotron source in the hard x-ray region of the spectrum.[5,6] Many authors have suggested that a sufficiently intense particle beam could generate stimulated emission.[6–11] Others have discussed pumping schemes which involve selective population of excited states via scattering.[9] All of these possible applications depend critically upon the detailed history of channeled particles as they propagate through a crystal.

A few determinations of occupation lengths have been made under widely different experimental conditions. Andersen *et al.* have measured the occupation length of axially channeled electrons in silicon in the energy range

of a few MeV.[12] Beezhold *et al.*[13] have determined the occupation length of planar channeled 54- and 83-MeV positrons in tungsten. Komaki *et al.*[14] obtained a $1/e$ occupation length of 31 μm for 350-MeV (110) planar channeled electrons in silicon. Also, Beloshitskii and Kumakhov[15] and Muralev[16] have calculated the dechanneling of axially channeled GeV electrons in silicon and tungsten.

In this paper we report the observation of CR emitted by 17-MeV electrons and 54-MeV electrons and positrons from silicon crystals of a wide range of thicknesses. By measuring the CR yields as a function of thickness, we have been able to deduce the dechanneling lengths and other details of the dechanneling process.

In Sec. II, we present the relevant theory of channeling and channeling radiation. In Sec. III, we develop a framework for relating the observed CR spectrum to the evolution of the channeled particles as they propagate and scatter through the crystal. In Sec. IV, we present some representative raw planar spectra and explain how we process these data to obtain the absolute CR flux as a function of thickness. In Sec. V, we use results from Sec. III and Sec. IV to derive detailed information about the channeled-particle population as a function of thickness. We conclude in Sec. VI with a discussion of the results and how the experimental arrangement could be modified or improved to yield more information about dechanneling and multiple scattering of channeled electrons and positrons.

II. RELEVANT THEORY OF CHANNELING AND CHANNELING RADIATION

For planar-channeled electrons and positrons with energies of less than about 100 MeV, the number of transverse energy levels in the continuum potential is small, and a quantal treatment is necessary. We use the many-beam method introduced for channeling-radiation calculations by Andersen *et al.*[12] to calculate eigenfunctions, energies, and spontaneous-emission cross sections.

As an example, the planar and thermally averaged potential for 54-MeV electrons channeled by the (100) plane of silicon is shown on the right-hand side of Fig. 1, along with the lowest transverse energy levels. This one-dimensional continuum potential governs the motion of electrons in the direction perpendicular to the plane (the $\hat{\mathbf{x}}$ direction.) Since the potential is periodic in the $\hat{\mathbf{x}}$ direction, the wave functions $u_n(x)$ can be expressed as Bloch waves with a band index n and a crystal momentum κ, where κ is confined to the first (one-dimensional) Brillouin zone. The left-hand side of Fig. 1 shows the details of the dependence of $\mathcal{E}_n$ upon κ. (κ is expressed as a fraction of g, the shortest reciprocal-lattice vector in the planar direction.) The energy bands are quite narrow for the lowest bound states because the wave functions are localized near the atomic nuclei, resulting in little overlap between adjacent wells.[6] Near the top of the well, the overlap between wave functions centered on adjacent wells becomes appreciable, and the energy bands acquire a noticeable width. Above the top of the well, the states are essentially plane waves, and the energy bands of these quasifree states broaden out to a near continuum which is punctuated by increasingly narrow energy gaps.

Channeling radiation consists of radiative transitions between the bound states. The CR photon energy is given, not by the difference in transverse energy $(\varepsilon_i-\varepsilon_f)$ between the two states, but approximately by $2\gamma^2(\varepsilon_i-\varepsilon_f)$—momentum conservation dictates that most of the photon energy is contributed by the longitudinal momentum of the particle. Radiative transitions between quasifree states are referred to as "coherent bremsstrahlung" (CB). More complete discussions of CR and CB are given in Refs. 17–19.

The spontaneous emission rate for a transition $i\rightarrow f$ is given by[17]

$$\frac{d^3N_{\mathrm{CR}}(i\rightarrow f)}{d\Omega_\gamma dE_\gamma dz}=\frac{\alpha\chi_c^2}{\pi\hbar c}\frac{E_\gamma}{2\gamma^2(1-\beta\cos\theta)}\left[\sin^2\phi+\left[\frac{\cos\theta-\beta}{1-\beta\cos\theta}\right]^2\cos^2\phi\right]|M_{fi}|^2\delta\left[E_\gamma-\frac{\mathcal{E}_i-\mathcal{E}_f}{1-\beta\cos\theta}\right], \tag{1}$$

where $d\Omega_\gamma$ is the differential solid angle of the observed photon, dz is the differential crystal thickness, and M_{fi} is the matrix element

$$M_{fi}=\left\langle u_f\left|e^{-iq_x x}\frac{d}{dx}\right|u_i\right\rangle\approx\left\langle u_f\left|\frac{d}{dx}\right|u_i\right\rangle. \tag{2}$$

(The approximate equality represents the usual dipole approximation, in which the $\hat{\mathbf{x}}$ component of the photon's wave vector, q_x, is set equal to zero.)

The linewidths can be calculated to a fair approximation with an optical-potential method.[20] The total spontaneous-emission spectrum is a sum of the individual spectral lines weighted by the populations of the initial states. This allows us to infer the populations of the states from the measured CR spectra. As will be demonstrated in Sec. V, the assumption that all states (bound *and* free) are populated equally yields calculated CR spectra which are in good agreement with spectra obtained from crystals of a wide range of thicknesses, allowing us to conclude that bound-state populations are approximately equal throughout the thickness of the crystal.

Although the measurement of CR spectra may seem to be a somewhat indirect method of obtaining occupation lengths, it is superior to methods which measure the energy-momentum distribution of the particle beam as it emerges from the crystal. When channeled particles emerge from the crystal, they are reconverted into free particles, and it is difficult to recover any information about the individual behavior of particles in different channeling states. This might be acceptable if there are

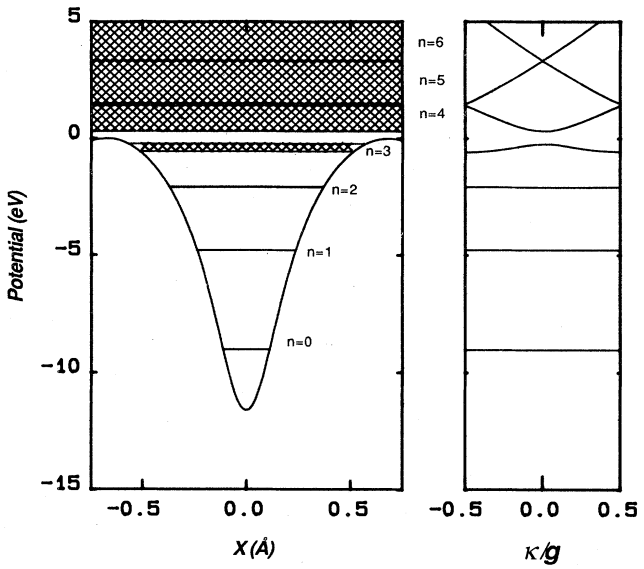

FIG. 1. Transverse energy levels of 54-MeV electrons channeled by the (100) planes of silicon. Transverse energy levels in the continuum potential well are indicated on the left; the full energy-band structure (reduced to the first Brillouin zone) is shown on the right. κ is the transverse crystal momentum and g is the magnitude of the shortest reciprocal-lattice vector in the (100) direction.

so many bound states that the channeled particles behave classically, as is the case for channeled ions or ultrarelativistic electrons or positrons. However, when the channeled particles are slow enough and/or light enough to behave quantum mechanically (as is the case for the experiments reported here), we would like to know about the detailed dynamics of particles in different channeling states. Since the CR is generated while the particles are channeling, these details are preserved in the CR spectra.

Given that the possibility of using CR as a spontaneous or perhaps a stimulated source of x rays and γ rays is a major motivation for studying occupation lengths, it is particularly appropriate to use CR to study them. In addition to possessing an intrinsic advantage over other methods of determining occupation lengths, measurements of CR from thick crystals reveal other aspects of the generation and properties of CR which must be understood before any practical use can be made of such a radiation source.

III. THE EFFECT OF MULTIPLE SCATTERING AND ABSORPTION UPON OBSERVED BREMSSTRAHLUNG AND CR SPECTRA

As a well-collimated beam of high-energy particles passes through a material, the particles undergo numerous small-angle collisions, resulting in a distribution of angles about the original direction. This "multiple-scattering" distribution has been determined theoretically and experimentally for *unchanneled* particles by a number of authors.[21–23] Our goal is to understand the behavior of *planar-channeled* particles as they pass through a crystal. In order to deduce this scattering behavior from our data, we must first derive expressions for the radiation spectra of beams of both unchanneled and planar-channeled particles in terms of their multiple-scattering distributions.

An unchanneled particle of initial plane-wave state $|\mathbf{k}_i\rangle$ will scatter repeatedly from the full electromagnetic potential of the solid through which it passes. Since the most likely transitions (both radiative and nonradiative) are small-angle deflections which have no perceptible effect on the energy of the particle, the longitudinal part of the motion need not be included explicitly in the representation of the particle's wave function. Thus a particle traveling at an angle Ω_e with respect to the forward direction may be represented by $|\Omega_e\rangle$. If a sufficient number of collisions have occurred, the particles perform a two-dimensional random walk around the forward direction, and their multiple-scattering distribution is approximately a two-dimensional Gaussian, with a standard deviation which increases roughly as the square root of the thickness. Several authors have derived an analytic form for $p(\Omega_e;z)$, the unchanneled particle distribution[21,22] as a function of the penetration depth z. The analysis is tractable because the states are plane waves and the populations may be represented by a single continuous function; nevertheless, it is quite difficult. Accurate formulas which are based upon theoretical analyses and fitted to experimentally determined parameters are given in Ref. 23. The distribution is, approximately,

$$p(\Omega_e;z)\approx\frac{1}{\pi\Theta_{\rm ms}^2(z)}e^{-\theta_e^2/\Theta_{\rm ms}^2(z)}, \tag{3}$$

where $\Theta_{\rm ms}(z)$ is the multiple-scattering angle and $\theta_e\equiv|\Omega_e|$. For the case of 54-MeV electrons in silicon, $\Theta_{\rm ms}(z)$ (mrad)$\approx 0.310z^{1/2}(2.32+1.12\ln z^{1/2})$, where the thickness z is expressed in μm.

The differential bremsstrahlung spectrum from unchanneled particles at penetration depth z can be calculated by convolving the multiple-scattering distribution of Eq. (3) with the differential bremsstrahlung flux for a thin target.[24] Near the forward direction,

$$\frac{d^3N_{\rm br}(\Omega_\gamma,E_\gamma)}{d\Omega_\gamma dE_\gamma dz}\propto E_\gamma^{-1}\frac{(1+\gamma^4\Omega_\gamma^4)}{(1+\gamma^2\Omega_\gamma^2)^4}, \tag{4}$$

where Ω_γ is the angle of the emitted photon with respect to the particle's direction and E_γ is the photon energy. The thick target bremsstrahlung spectrum is then obtained by integrating this convolution over z, taking photon absorption into account.

The results of this calculation for 54-MeV e^- in silicon are displayed in Fig. 2. This curve is very nearly independent of the beam energy because the multiple-scattering angle and the characteristic width of the angular distribution of bremsstrahlung both scale as $1/\gamma$. The standard thin-target bremsstrahlung formula can be multiplied by this curve to obtain the total flux emitted in the forward direction from a material of thickness Z. Note that the bremsstrahlung production increases linearly with thickness at first, but starts to saturate noticeably

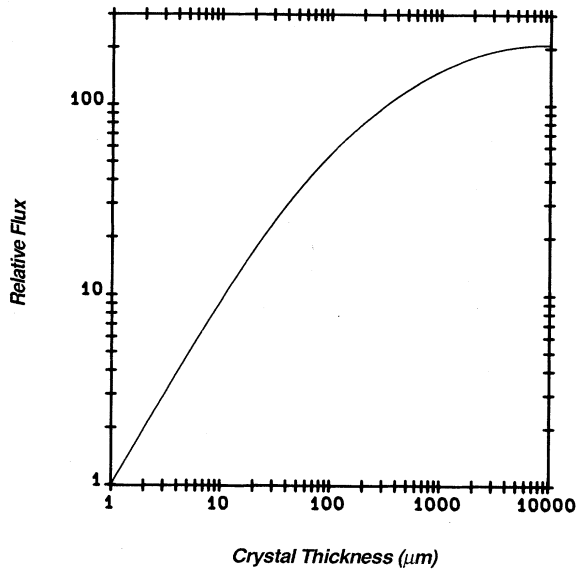

FIG. 2. Calculated bremsstrahlung flux of photons with energies between 80 and 100 keV emitted in the forward direction by randomly-directed relativistic electrons or positrons in thick silicon targets, normalized to the corresponding thin-target bremsstrahlung flux per micron.

near 50 μm, at which point $\Theta_{\rm ms}$ becomes comparable to $(2\gamma)^{-1}$.

It is reasonable to assume that, like unchanneled particles, planar-channeled particles lose very little of their forward momentum as they pass through a crystal (provided that its thickness is much less than the radiation length, which is so in all reasonable cases). Therefore, the wave function of a planar-channeled particle in the nth energy band with wave-vector κ traveling at an angle θ_e with respect to the forward direction can be represented by $|n\kappa\theta_e\rangle$, and the multiple-scattering distribution can be denoted $p_n(\kappa,\theta_e;z)$. $p_n(\kappa,\theta_e;z)$ differs in two significant ways from its analog for unchanneled particles, $p(\Omega_e;z)$. First, channeled particles scatter only from those components of the crystal's electromagnetic potential which fluctuate in space and time, since the static continuum potential is already taken into account in the calculation of the channeling states. Also, for channeled particles, multiple scattering is confined to the θ direction (parallel to the channeling planes and perpendicular to the forward direction). In the other transverse direction (perpendicular to the planes), scattering takes the form of transitions $|n_i\kappa_i\rangle \rightarrow |n_f\kappa_f\rangle$ between discrete bound states rather than between two states in a continuum.

Our objective is to learn as much as possible about $p_n(\kappa,\theta_e;z)$ by measuring the radiation spectrum of a beam of multiply scattered channeled particles. However, little can be learned about the dependence of $p_n(\kappa,\theta_e;z)$ upon the wave-vector κ because the energies of the bound states are insensitive to κ (which is precisely why CR consists of prominent spectral lines). It is consoling to realize that the dependence of $p_n(\kappa,\theta_e;z)$ upon κ is probably rather uninteresting anyway; the population within a band is expected to equilibrate on a time scale much faster than the rate at which the total population of the band changes. This is due to the fact that, since the energies within a band are almost degenerate, the intraband scattering rate ought to be much faster than the interband scattering rate. Thus it is sufficient to measure $p_n(\theta_e;z)$, the population distribution integrated across the band. $p_n(\theta_e;z)$ can be thought of as the product of two functions: $p_n(z)$, which describes the evolution of the total population within a band n and from which the occupation length may be extracted, and $f_n(\theta_e;z)$, a *one*-dimensional multiple-scattering distribution function normalized so that its integral over θ_e is unity.

Currently, very little is known about the multiple-scattering distribution $f_n(\theta_e;z)$ for channeled particles. However, it is probably reasonable to assume that its form is similar to that for unchanneled particles (Gaussian), with some multiple-scattering angle $\Theta_n(z)$ which depends upon the band index n. The multiple-scattering angles $\Theta_n(z)$ are almost certainly different from one another and from $\Theta_{\rm ms}(z)$. Unfortunately, it is difficult to relate $\Theta_n(z)$ to $\Theta_{\rm ms}(z)$. Channeled electrons are more concentrated in the vicinity of the nuclei, resulting in increased scattering, while channeled positrons are less concentrated, resulting in suppressed scattering. To a first approximation, the enhancement (or suppression) ought to be given by the square of the magnitude of the wave function evaluated at the position of the nuclei. However, it is still difficult to relate this enhancement or suppression to $\Theta_n(z)$ because the scattering processes couple the different functions $f_n(\theta_e;z)$ to one another. If the CR peaks are sufficiently well separated, it might be possible to determine the multiple-scattering angles for the different bound states experimentally by examining the line shapes in detail.

The radiation spectrum of a beam of channeled particles passing through a target of thickness Z is given by the convolution of the differential CR cross section with the multiple-scattering distribution

$$\frac{d^2N_{\rm CR}(i\rightarrow f)}{dE_\gamma d\Omega} = \frac{d^3N_{\rm CR}(i\rightarrow f)}{dE_\gamma d\Omega_\gamma dz} \otimes \int_0^z dz\, p_i(\theta_e;z)e^{-\mu E_\gamma(Z-z)} \quad (5)$$

The exponential factor in the integral accounts for self-absorption of photons in the target, and $\mu(E_\gamma)$ is the absorption coefficient of photons with energy E_γ. The thin-target channeling radiation flux $d^3N_{\rm CR}(i\rightarrow f)(\Omega_\gamma,E_\gamma)/d\Omega_\gamma dE_\gamma dz$ is given by Eq. (1). Note that the relationship between the radiation spectrum of a beam of channeled particles and its population distribution $p_n(\theta_e;z)$ is more complicated than the corresponding relationship for unchanneled particles. One obvious complication in Eq. (5) is the existence of several separate continuous functions which are required to describe the population distributions—one for each band n. A second complication is the fact that the radiation intensity distribution $d^3N_{\rm CR}(i\rightarrow f)(\Omega_\gamma,E_\gamma)/d\Omega_\gamma dE_\gamma dz$ depends upon the transition $i\rightarrow f$ and is not separable in the variables Ω_γ and E_γ, as was the function

$d^3N_{\rm br}(i\rightarrow f)(\Omega_\gamma,E_\gamma)/d\Omega_\gamma dE_\gamma dz$ for unchanneled particles [compare Eqs. (1) and (4)]. More specifically, the CR peak resulting from a transition from a state with discrete index n_i to one with an index n_f is centered at $(\mathcal{E}_i-\mathcal{E}_f)/(1-\beta\cos\theta_\gamma)$, where $\beta=(1-\gamma^{-2})^{-1/2}$ and θ_γ is the angle between the particle direction and the direction of the emitted photon.[5] Thus, the energies of photons emitted in a particular direction will depend upon the direction θ_γ as well as the indices n_i and n_f. If the incident particle beam has some divergence or if multiple scattering occurs, the CR peaks will lose intensity and become asymmetric (broader on the lower-energy side). As will be discussed further in Sec. V E, the multiple-scattering angles $\Theta_n(Z)$ can in principle be determined from the asymmetric distortion and slight downward shift of the channeling radiation peaks.

Fortunately, Eq. (5) can be simplified if the population is distributed evenly throughout each band and the multiple-scattering angle Θ_i is sufficiently small compared to $1/\gamma$ over the range through which $p_i(z)$ is significant (so that multiple scattering can be neglected), in which case Eq. (5) simplifies to

$$\frac{d^2N_{\rm CR}(i\rightarrow f)}{dE_\gamma d\Omega}=\frac{d^3N_{\rm CR}(i\rightarrow f)}{dE_\gamma d\Omega_\gamma dz}\int_0^z dz\, p_i(z)e^{-\mu(E_\gamma)(Z-z)} \tag{6}$$

in the forward direction. If the individual CR peak pertaining to a transition $i\rightarrow f$ can be resolved, the integral $\int_0^z dz\, p_i(z)\exp[\mu(E_\gamma)z]$ can be obtained by dividing the measured value of $d^2N_{\rm cr}(i\rightarrow f)/dE_\gamma d\Omega$ by the calculated value of $[d^3N_{\rm CR}(i\rightarrow f)(\Omega_\gamma,E_\gamma)/d\Omega\gamma dE_\gamma dz]\times\exp[\mu(E_\gamma)Z]$. Thus $p_i(z)$, the dependence of the total population within the ith band upon thickness, can be constructed by measuring $d^2N_{\rm CR}(i\rightarrow f)/dE_\gamma d\Omega$ for several different crystal thicknesses.

IV. DATA PROCESSING

The measurements were performed with beams of 17-MeV electrons and 54-MeV electrons and positrons at the Lawrence Livermore National Laboratory Electron-Positron Linear Accelerator. The experimental apparatus and procedures are described in Ref. 6.

Unprocessed CR spectra produced by 54-MeV electrons channeled by the (100) plane of silicon for four different crystal thicknesses are displayed in Figs. 3(a)–3(d). The three peaks constitute the CR. The smooth background is due mainly to bremsstrahlung, with a smaller contribution from coherent bremsstrahlung (CB). Thus, the relative magnitudes of the peaks and the background are related to the proportion of channeled particles. In Fig. 3, the decrease in the peak-to-background ratio with increasing thickness is readily apparent. It appears that the bound-state populations at 2.8 and 19 μm are roughly equal, and that they decrease to less than half of their original value somewhere between 19 and 130 μm. At a thickness of 2765 μm, the CR peaks are greatly diminished, but still perceptible.

Representative unprocessed spectra produced by 54-MeV positrons channeled by the (110) plane of silicon for four different thicknesses are displayed in Figs. 4(a)–4(d). The peak-to-background ratio diminishes slightly between 19 and 94 μm, and substantially between 94 and 1200 μm—indicating a half-length somewhere between 19 and 94 μm. Despite the strong absorption of low-energy photons by the crystal, the positron CR peak is still quite strong relative to the background even when the crystal is nearly 1-cm thick.

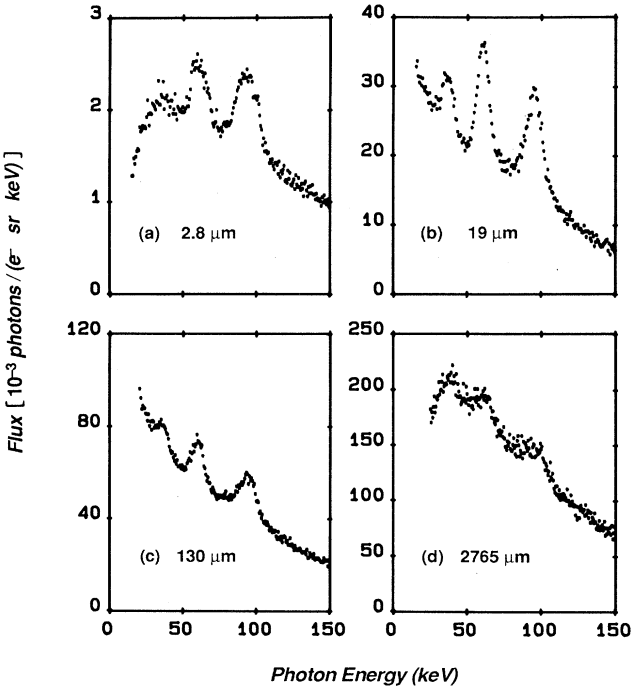

FIG. 3. Raw spectra obtained from 54-MeV electrons channeled by the (100) plane of silicon for four different crystal thicknesses: (a) 2.8 μm, (b) 19 μm, (c) 130 μm, and (d) 2765 μm.

These spectra demonstrate qualitatively the depopulation of transverse bound states. However, for a quantitative analysis, several factors must be taken into account. For example, the total beam charge was different in each case. A different detector was used for the 2.8-μm electron spectrum. As described in Sec. III, the effect of absorption and multiple scattering on both the bremsstrahlung and the CR must be accounted for properly.

The raw spectra were collected and then processed according to the following procedure, which is described in fuller detail in Ref. 25. First, for each plane, we took a planar channeling spectrum and an accompanying "random" spectrum (obtained by tilting the crystal away from the planar direction so that only ordinary bremsstrahlung was produced). For both spectra, the total beam charge was measured by a plastic scintillator and photomultiplier placed in the beam dump. Pileup, which was held to, at most, 15% during the experiment, was removed from all spectra by a computer algorithm which has been tested against experimental spectra taken at low and high counting rates. The spectra were then corrected for escape of 9.9-keV Ge $K\alpha$ x rays from the Ge detector.

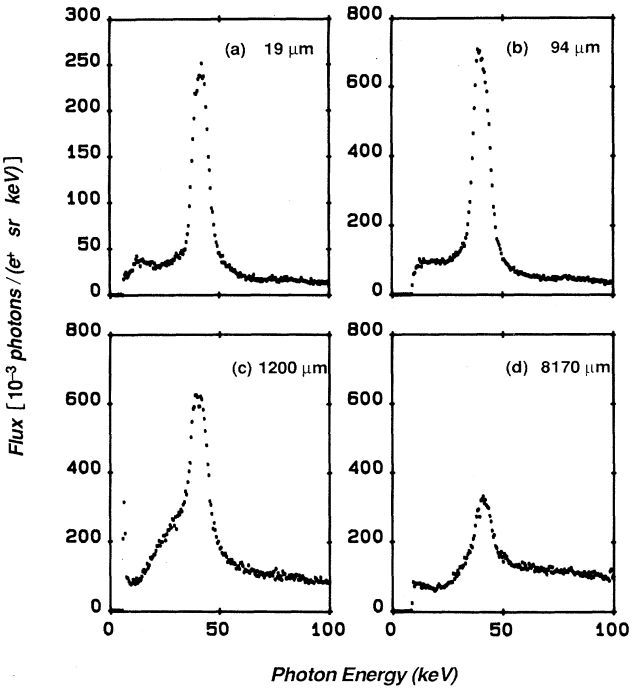

FIG. 4. Raw spectra obtained from 54-MeV positrons channeled by the (110) plane of silicon for four different crystal thicknesses: (a) 19 μm, (b) 94 μm, (c) 1200 μm, and (d) 8170 μm.

This was particularly important for the 17-MeV electron Si(100) data, which contains a noticeable escape peak from the 13-keV $1\rightarrow 0$ transition.

After these initial data-processing steps, we subtracted from each planar spectrum a constant times its corresponding random spectrum. The constant was chosen so as to give the best fit in the energy range from 10 to 200 keV. The value of this constant is typically between 1.0 and 1.2 for electrons and about 1.0 for positrons. Considering that channeled electrons are localized near the atomic nuclei, it is surprising that their bremsstrahlung intensity is not enhanced significantly over that of randomly directed electrons; nor is the bremsstrahlung intensity from channeled positrons reduced significantly below that of randomly directed positrons. (A similar experimental result is reported and discussed in Ref. 19.) The resultant subtracted spectrum is then divided by a detector efficiency calibration curve obtained by calibration against bremsstrahlung spectra and radioactive sources[26] and by correction of the manufacturer's published values of the detector efficiency[27] for absorption in the windows[28] and in air.[26]

The absolute CR yield in units of photons/sr/keV is established by calibrating to the bremsstrahlung yield between 80 and 100 keV from a randomly oriented crystal. As discussed in Sec. III, the thin-target bremsstrahlung yield[29] must be corrected for multiple scattering of the particle beam and photon absorption in the target. This spectral region has been chosen for several reasons—very little absorption takes place until the crystal thickness exceeds 1 mm, the detector efficiency is nearly 100%, and pileup and noise are minimal. The bremsstrahlung differential cross section in the forward direction for silicon is $d^3N_{\rm br}(\Omega_\gamma,E_\gamma)/d\Omega_\gamma dE_\gamma dz = 4.07\times 10^{-6}\gamma^2/(\mu{\rm m\,sr}\,e^{-,+})^{-1}$. Therefore, the total number of bremsstrahlung photons emitted per 54-MeV electron or positron with energy between 80 and 100 keV is $d^2N_{\rm br}(\Omega_\gamma)/d\Omega_\gamma dz = 1.05\times 10^{-2}\ (\mu{\rm m\,sr}\,e^{-,+})^{-1}$. Multiplying $d^2N_{\rm br}(\Omega_\gamma)/d\Omega_\gamma dz$ by the thick-target curve displayed in Fig. 2 yields $dN_{\rm br}(\Omega_\gamma,Z)/d\Omega_\gamma$, the total bremsstrahlung flux per steradian per particle in the forward direction for a crystal of thickness Z.

After a preset amount of charge has been collected by the beam-dump scintillator after passing through a randomly aligned crystal, we collect N_γ photons in the spectral range 80–100 keV, from which we can determine the product $\delta\Omega_\gamma N(e^{-,+}) = N_\gamma/[dN_{\rm br}(\Omega_\gamma,Z)/d\Omega_\gamma]$. If a planar spectrum is taken under identical experimental conditions (i.e., the collimators, the detector, and the beam profile and divergence are unchanged and the same amount of charge is collected by the scintillator), we may assume that this product is the same for the CR spectrum. Therefore, the CR flux per particle per solid angle per unit energy for photons with energy E_i is given by $d^2N_{\rm CR}(i\rightarrow f)(\mathbf{0},E_i)/d\Omega_\gamma dE_\gamma = s_i/[N(e^{-,+})\delta\Omega_\gamma\delta E]$, where δE is the energy interval per bin of the multichannel analyzer and s_i is the number of photons in the ith energy bin. This yields a subtracted, processed, normalized planar spectrum in units of photons/($e^{-,+}$sr keV).

Finally, to extract populations and occupation lengths, we integrate the CR intensity in some appropriate region of the spectrum and then divide the measured intensity by the calculated dipole transition strength $d^2N_{\rm CR}(n_i\rightarrow n_f)(\mathbf{0},E_\gamma)/d\Omega_\gamma dz$ of Eq. (1) to obtain the integral $\int_0^Z p_{n_i}(z)e^{-\mu(E_\gamma)(Z-z)}dz$ [see Eq. (6)]. For 54-MeV electrons or positrons in silicon,

$$d^2N_{\rm CR}(i\rightarrow f)(\mathbf{0},E_\gamma)/d\Omega_\gamma dz(e^{-,+}\ {\rm sr}\ \mu{\rm m})^{-1} = 1.76\times 10^{-4}E_\gamma({\rm keV})|M_{\rm if}\ ({\rm \AA}^{-1})|^2\ ,$$

where $E_\gamma = (\mathcal{E}_i-\mathcal{E}_f)/(1-\beta\cos\theta)\approx 2\gamma^2(\mathcal{E}_i-\mathcal{E}_f)$ in the forward direction.

V. EXPERIMENTAL RESULTS

A. Introduction

As an example, the spectra of Figs. 3(a)–3(d) [54-MeV electrons channeled by the (100) planes of silicon] and Fig. 4(a)–4(d) [54-MeV positrons channeled by the (110) planes of silicon] have been processed according to the procedures described in Sec. IV and displayed in Figs. 5(a)–5(d) and 6(a)–6(d). For comparison, the corresponding calculated CR spectra are superimposed on Figs. 5(b) and 6(a), respectively. Multiple scattering has not been included in the calculation; this would tend to meld the sharp spikes of Fig. 6(a) into the observed composite peak of Figs. 6(a)–6(d). The distribution of population within each band is assumed to be uniform in κ and a delta function in θ. For purposes of normalization (to

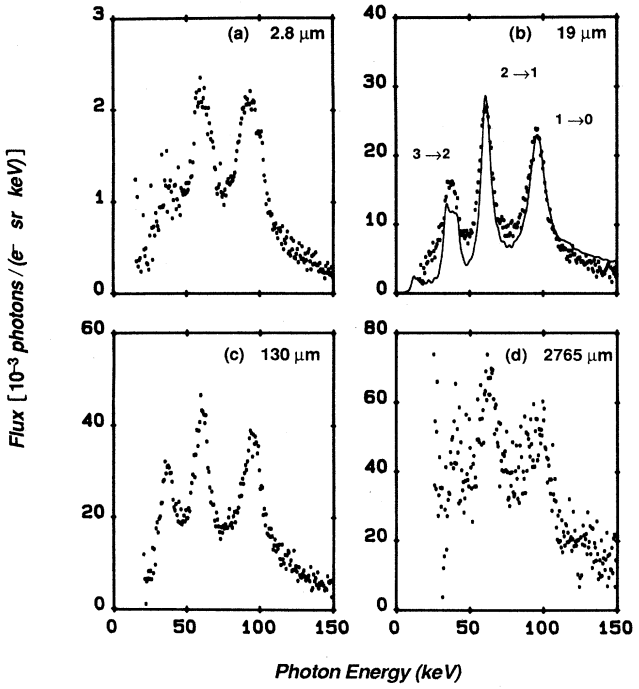

FIG. 5. Processed CR spectra obtained from 54-MeV electrons channeled by the (100) plane of silicon for four different crystal thicknesses: (a) 2.8 μm, (b) 19 μm (with calculated CR spectrum superimposed), (c) 130 μm, and (d) 2765 μm.

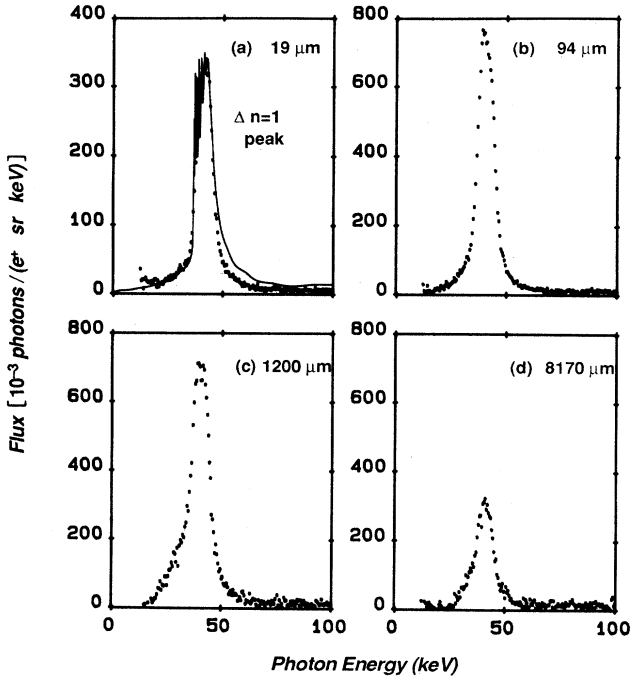

FIG. 6. Processed spectra obtained from 54-MeV positrons channeled by the (110) plane of silicon for four different crystal thicknesses: (a) 19 μm (with calculated CR spectrum superimposed), (b) 94 μm, (c) 1200 μm, and (d) 8170 μm.

a delta function in θ. For purposes of normalization (to be explained below), it is assumed that the total population within each of the energy bands is 100%.

These assumptions about the population distribution require some explanation. It is not unreasonable to assume that the populations of the bound and free states are equal. As will be seen in Secs. V B, V C, and V D, a Gaussian beam with a divergence larger than about 0.2 to 0.5 mrad will populate the bound states almost equally. Even if the populations are initially unequal, a detailed-balance argument would lead one to expect a tendency towards an equilibrium in which all states are populated equally. Perfect equilibrium is never reached because the particles spend a finite amount of time in the crystal, but one might expect the populations of states with sufficiently small transverse energies to be approximately equal in sufficiently thick crystals.

Detailed calculations reveal that the lower-energy free states contribute a smooth background of CB in the spectral region where CR is most prominent. Free states with energies which are well up in the continuum, which are less likely to be populated unless the crystal is sufficiently thick, contribute very little CB in the spectral region of interest. Therefore, it does not matter if the equal-population approximation is not strictly valid for the free states. The assumption of 100% population in each band is clearly a physical impossibility; it is merely a convenient normalization which allows the populations to be determined directly from Eq. (6).

Since intraband scattering is more rapid than interband scattering, the assumption of a uniform distribution in κ is consistent with the assumption of equal populations in each band. However, the assumption that all particles are traveling in the direction $\theta=0$ is inconsistent with the assumption that the initial beam divergence and/or scattering has been sufficient to populate the bands equally. Nevertheless, multiple scattering in the θ direction has a much smaller effect on the observed spectrum than scattering in the x direction, for two reasons. First, the effect of beam divergence and/or scattering in the x direction is to distribute population in the bands, thereby determining the intensity of the transitions. On the other hand, beam divergence and/or multiple scattering in the θ direction serves only to distort the spectrum via the Doppler shift. Second, the characteristic transverse-momentum scales are different in the x and θ directions. In the x direction, the classical critical angle (the angle of incidence below which most of the particles will be captured into bound states) is $\theta_c=2(V_{\max}/E)^{1/2}$, where $V_{\max}$ is the depth of the planar-averaged transverse potential (about 15 to 25 eV for the major planes of silicon) and E is the energy of the incident beam. This gives a critical angle of about 1.0 to 1.4 mrad for 54-MeV particles. In the θ direction, the photon energy is approximately proportional to $1/[1+(\theta\gamma)^2]$ [Eq. (1)], where $\gamma=107.6$, so that divergence in the θ direction becomes important on a scale of about 10 mrad, which is considerably larger than the critical angle. Moreover, the effect of any Doppler broadening which *does* occur is mitigated by the fact that the it is the *integrated* intensity of each peak which is measured. For these reasons, one would

expect the calculated spectra to bear a reasonably close resemblance to the observed spectra.

A glance at Fig. 5 reveals that the 54-MeV electron (100) spectra are qualitatively similar to the calculated spectra. The CR peaks are noticeably broader in the 2.8-μm spectrum; the crystal is so thin that the lifetime broadening due to finite crystal thickness is significant (see Refs. 5 and 17 for a fuller discussion of this effect.) The 19- and 130-μm spectra have much the same shape as the calculated spectrum, but there are some notable differences. In the 19-μm spectrum, the CB background appears to be weaker than that calculated. This might indicate that the average population of the free states between 0 and 19 μm is not yet comparable to that of the bound states. In support of this hypothesis, the CB background appears to be slightly stronger in the 130-μm spectrum, which matches the calculated spectrum quite well. Although it is difficult in general to distinguish between unbroadened CR peaks sitting on an augmented background and broadened CR peaks sitting on an unaugmented background, the failure of the centroids of the CR peaks to shift downward by a discernible amount between the 19- and 130-μm spectra suggests that multiple scattering is unimportant and that the differences between the two spectra may be attributed to an increased CB background. The relative intensities of the CR peaks (and hence the relative integrated populations of the $n=1$, $n=2$, and $n=3$ states) are approximately equal in the 19- and 130-μm spectra. The absolute intensity of CR increases very litle between 19 μ and 130 μm, indicating that the bound states have lost a significant fraction of their population after penetrating 19 μm. It appears that some more CR may be generated between 130 and 2765 μm, but uncertainties in the background subtraction due to poor statistics and in the thick-target bremsstrahlung calculations for extremely thick samples preclude a definite statement.

B. 54.5-MeV electron data

It is difficult to separate quantitatively the individual peaks in Figs. 5(a)–5(d). However, since the observed spectra seem to support the claim that all bound states are approximately equally populated, the theoretical and observed absolute yields will be compared in a spectral region which covers several of the CR peaks. In Fig. 7, the measured channeling-radiation yield of 54.5-MeV electrons channeled by the (100) planes of silicon between 50 and 110 keV (covering the energy region of the $1\rightarrow 0$ and $2\rightarrow 1$ peaks) is plotted as a function of crystal thickness, along with two fitted curves. The fairly large scatter in Fig. 7 arises from several sources, including the uncertainty in the background subtraction and that in the bremsstrahlung normalization. Another source of scatter is the fact that the beam divergence, and hence the initial population distribution, varied somewhat because the data were collected in a series of experimental runs spanning three years. Different symbols represent different beam conditions. The absorption correction factor $\exp[\mu(E_\gamma)Z]$ of Eq. (6) is significant only for crystal thicknesses greater than 1000 μm. For thicknesses

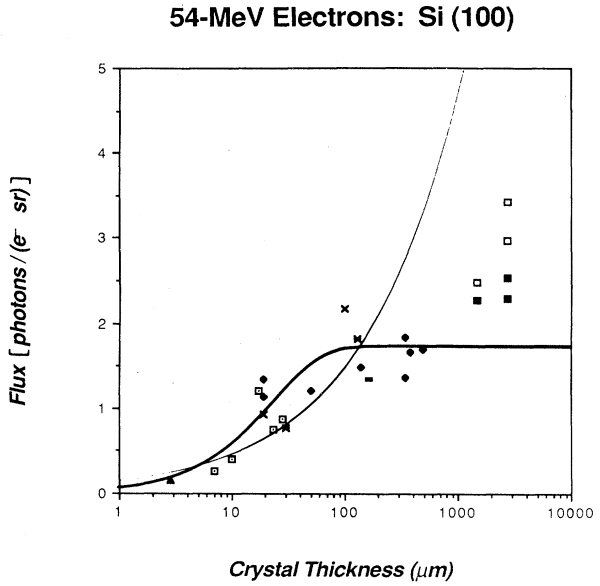

FIG. 7. Measured CR flux in the spectral region between 50 and 100 keV from 54-MeV electrons channeled by the (100) plane of silicon as a function of crystal thickness. The different symbols represent different experimental conditions. For thicknesses greater than 1000 μm, the absorption-corrected fluxes are represented by open squares. The "multiple-scattering" fit, $0.15Z\ (\mu\text{m})^{1/2}$, is represented by the thin solid curve; the "integrated-exponential" fit, $1.75\ (1-e^{-Z(\mu\text{m})/24})$, is represented by the thick solid curve.

greater than 1000 μm, the measured yields must be corrected for photon self-absorption.

As was stated in Sec. V A, the calculated yield is based upon the assumption that each level has a population of 100%. Thus, from Eq. (6), the integrated population $\int_0^Z dz\, p_{n_i}(z)\exp[\mu(E_\gamma)z]$ may be obtained by dividing the corrected yield in photons/($e^{-,+}$ sr) by the calculated yield in photons/(sr $e^{-,+}\mu$m.)

For thicknesses less than 500 μm, the points appear to fit an integrated exponential (of the form $A[1-\exp(-Z/L_{\text{occ}})]$) reasonably well. Since the absorption correction factor is negligible for such thicknesses, the population $p_{n_i}(z)$ is essentially equal to the derivative of the corrected yield plotted in Fig. 7. From this, a $1/e$ length L_{occ} of 24 μm for 54-MeV electrons channeled along Si(100) is obtained. The slope of this curve at 0 thickness is 0.073 photons/e^- sr μm), as compared to the calculated flux (based upon 100% population in each state) of 0.89 photons/(e^- sr μm), giving an initial population of 8.2% in both the $n=1$ and the $n=2$ levels.

The integrated-exponential curve underestimates the measured yield for crystals thicker than 1000 μm. This may indicate that the population decay is slower than exponential for sufficiently thick crystals. In the classical limit (in which there is a continuum of transverse energy levels) one would expect the dependence of population upon penetration depth to behave like multiple scatter-

ing, i.e., proportional to $Z^{-1/2}$. A curve of the form $AZ^{1/2}$ has been fitted to the data in Fig. 7, but it overestimates the yield for thick crystals. This might indicate that the population decay rate lies somewhere between the exponential and multiple-scattering extremes. Another possibility is that the measurements of photon flux from crystals thicker than 1 mm are unreliable. There are three important sources of uncertainty in the data from extremely thick crystals: the calculation of thick-target bremsstrahlung upon which the flux normalization is based may not be very accurate for extremely thick crystals, the background subtractions are subject to greater uncertainty with increasing thickness, and a different, extremely-low-intensity electron beam was used for the very thick crystals.

A typical CR spectrum for 54-MeV electrons channeling along the (110) plane of silicon is presented in Fig. 8, and the CR yields as a function of crystal thickness for that plane are displayed in Fig. 9. Since there are six $\Delta n = 1$ transitions for (110) as compared to three for the (100), it is even more difficult to separate the individual CR peaks from one another. However, a calculation of the (110) spectrum [based upon the same assumptions about population distribution that were made for the (100) calculation] is in good agreement with the observed spectra. Therefore, as was done for the (100) plane, the measured and calculated channeling-radiation spectra are compared in some spectral region (55 to 140 keV) which spans several of the CR peaks (the $1 \rightarrow 0$, $2 \rightarrow 1$, and $3 \rightarrow 2$ peaks) to obtain Fig. 9. The $1/e$ length for the (110) plane is about 50% greater than that for the (100) plane—about 36 μm. The slope of the population curve is about 0.10 photons/(e^- sr μm) at 0 μm, while the calculated flux is 2.3 photons/(e^- sr μm), implying an initial population of 4.3% in each of the $n = 1$, 2, and 3 levels.

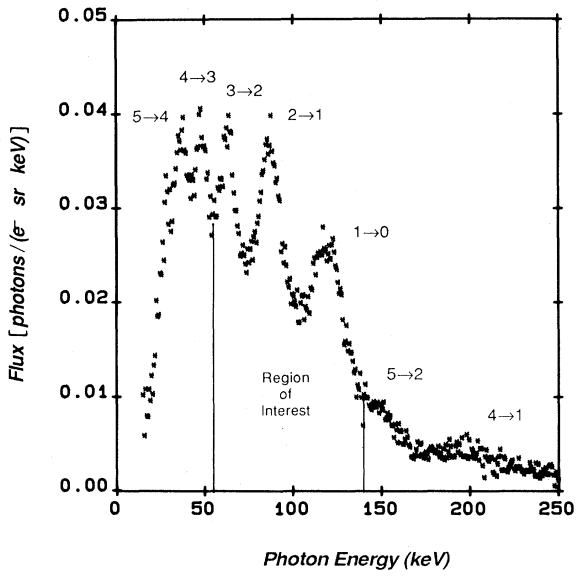

FIG. 8. Observed CR spectrum from 54-MeV electrons channeled by the (110) plane of a 19-μm-thick silicon crystal. The spectral region of interest (55 to 140 keV) is demarcated by vertical lines.

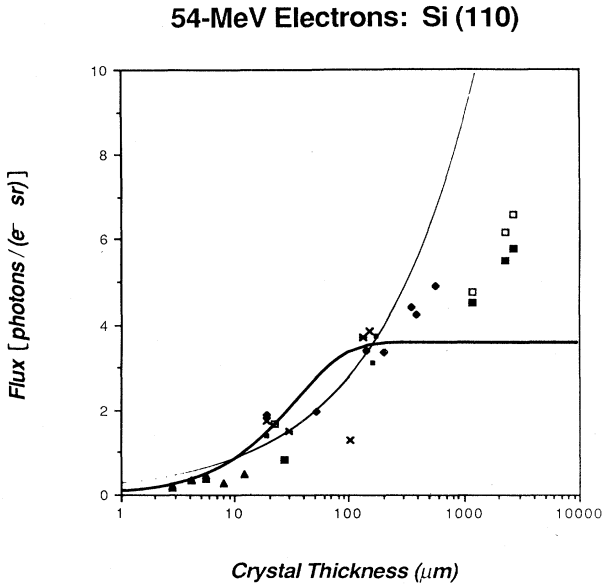

FIG. 9. Measured CR flux in the spectral region between 55 and 140 keV from 54-MeV electrons channeled by the (110) plane of silicon as a function of crystal thickness. The different symbols represent different experimental conditions. Open squares have the same interpretation as in Fig. 7. The "multiple-scattering" fit, $0.28Z$ $(\mu m)^{1/2}$, is represented by the thin solid curve; the "integrated-exponential" fit, 3.6 $(1-e^{-Z(\mu m)/36})$, is represented by the thick solid curve.

Figures 10(a) and 10(b) display calculated bound-state initial populations as a function of beam divergence for 54.5-MeV electrons for the (100) and (110) planes, respectively. The divergence of 54.5-MeV electron beams in the

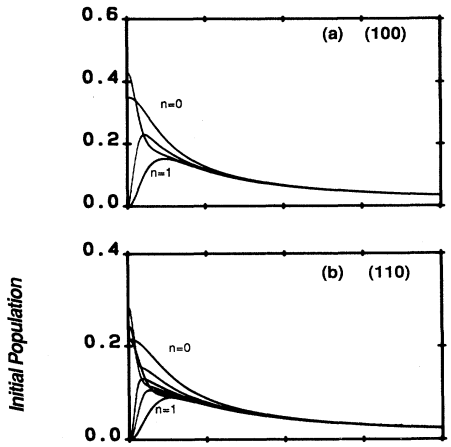

FIG. 10. Calculated bound-state initial populations as a function of electron-beam divergence for 54-MeV electrons channeled by (a) the (100) plane and (b) the (110) plane of silicon.

experiments is typically of the order of 1 mrad or less. At 1 mrad, the calculated initial populations of the bound states are in the range of about 6–7 % for the (100) plane and 4–5 % for the (110) plane, which agrees well with the measured values of 8.2% and 4.3%, respectively.

C. 54.5-MeV positron data

For 54.5-MeV positrons, the $\Delta n = 1$ peaks lie almost on top of one another. For all three major planes, the shape of the experimental peak is quite close to that given by the calculation. The very fine structure in the calculated peak of Fig. 6(a) is not observed in the data because of multiple scattering and other line-broadening effects which were not taken into account in the calculation.

Since the individual peaks cannot be resolved, the analysis must be based again upon some spectral region which includes several peaks. The shape of the composite peak matches that of the observed one rather well. Therefore, the usual assumption that the individual states are equally populated is made. Unfortunately, the positron CR peaks extend as low as 20 keV, where the absorption is quite severe for crystals thicker than a few hundred microns. Application of the absorption correction at the low-energy side of the peak magnifies statistical noise and spurious sources of radiation, resulting in greater uncertainty in the absorption-corrected fluxes of the thicker crystals.

Figures 11–13 display the measured fluxes of the (100),

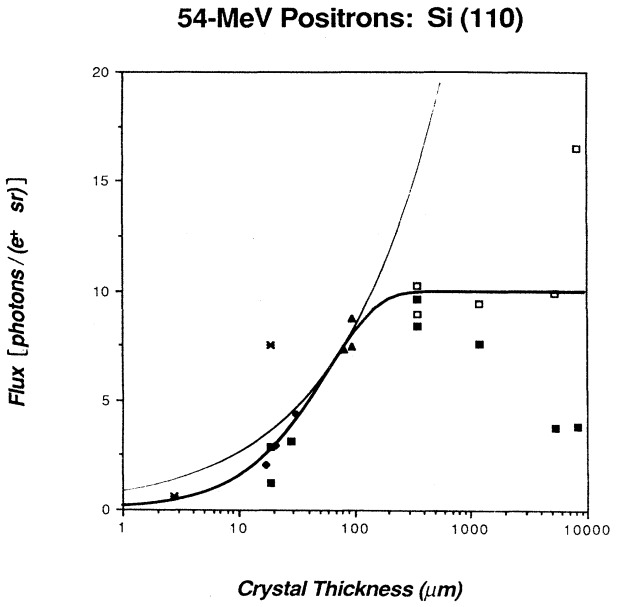

FIG. 12. Measured CR flux in the $\Delta n = 1$ peak for 54-MeV positrons channeled by the (110) plane of silicon as a function of crystal thickness. The different symbols represent different experimental conditions. Open squares have the same interpretation as in Fig. 11. The "multiple-scattering" fit, $0.83Z\ (\mu m)^{1/2}$, is represented by the thin solid curve; the "integrated-exponential" fit, $10\ (1-e^{-Z(\mu m)/60})$, is represented by the thick solid curve.

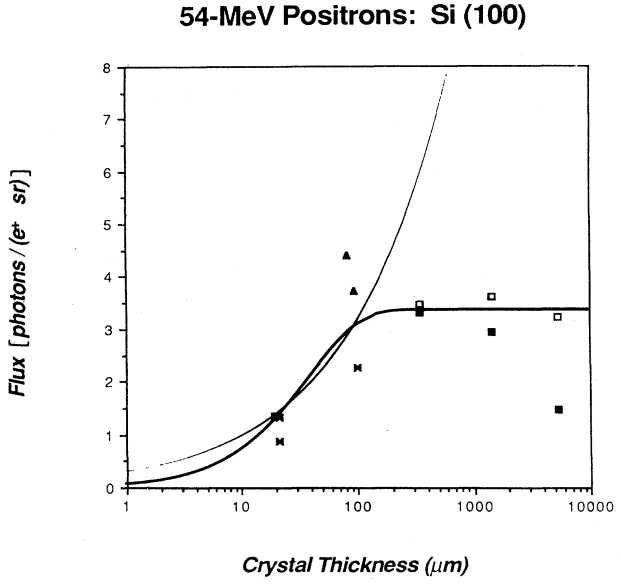

FIG. 11. Measured CR flux in the $\Delta n = 1$ peak for 54-MeV positrons channeled by the (100) plane of silicon as a function of crystal thickness. The different symbols represent different experimental conditions. For thicknesses greater than 200 μm, the absorption-corrected fluxes are represented by open squares. The "multiple-scattering" fit, $0.32Z\ (\mu m)^{1/2}$, is represented by the thin solid curve; the "integrated-exponential" fit, $3.4\ (1-e^{-Z(\mu m)/40})$, is represented by the thick solid curve.

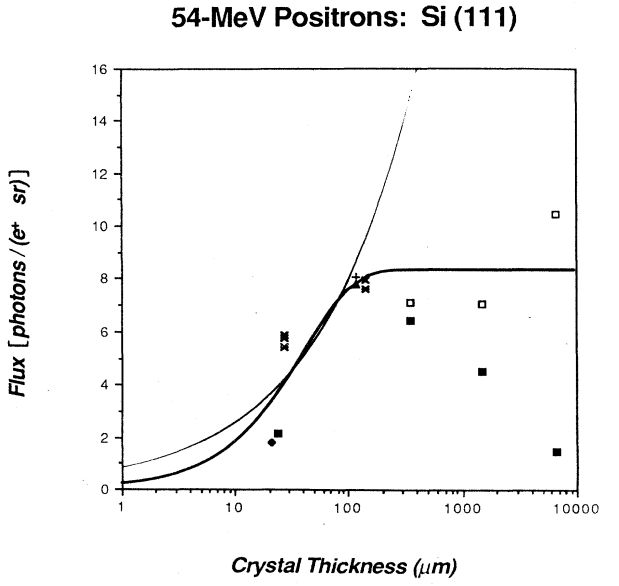

FIG. 13. Measured CR flux in the $\Delta n = 1$ peak for 54-MeV positrons channeled by the (111) plane of silicon as a function of crystal thickness. The different symbols represent different experimental conditions. Open squares have the same interpretation as in Fig. 11. The "multiple-scattering" fit, $0.80Z\ (\mu m)^{1/2}$, is represented by the thin solid curve; the "integrated-exponential" fit, $8.4\ (1-e^{-Z(\mu m)/42})$, is represented by the thick solid curve.

(110), and (111) peaks. For crystal thicknesses greater than a few hundred microns, the absorption correction factor $\exp[\mu(E_\gamma)Z]$ of Eq. (6) has been included. In the most extreme instance [the 0.817-cm-thick (110) plane], this factor is slightly over 4. As in the case of electrons, the derived occupation length is sufficiently short that the thickness through which the absorption occurs can be taken to be the full thickness of the crystal, i.e., neglect of the exponential factor in the integral of Eq. (6) is a good approximation.

Exponential fits to the positron data in Figs. 11–13 yield $1/e$ lengths of 40, 60, and 42 μm for the (100), (110), and (111) planes. The exponential fits appear to be much better for the positron data than they were for the electron data of Figs. 7 and 9. The slopes of the population curves are 0.085, 0.167, and 0.200 photons/(e^+ sr μm), respectively. The calculated fluxes for these three planes are 1.6, 6.1, and 7.8 photons/(e^+ sr μm), giving initial populations of 5.3% in each of six bound states for the (100), 2.8% in each of 12 bound states for the (110), and 2.5% in each of 17 bound states for the (111) plane. The measured initial populations of all three planes are consistent with a beam divergence of about 1.0–1.4 mrad.

One anomaly in the positron data merits attention. In Fig. 12, one of the 19-μm (110) positron peaks is over twice as intense as the other 19-μm (110) peaks; in fact, it rivals the 100-μm peaks in intensity. For this particular spectrum, the population in each bound state (averaged over the thickness of the crystal) must have been 6.4% in each of the 12 bound states—about 75% of the positrons were channeled. Taking the occupation length of 60 μm into account, the initial population in each bound state must have been 7.5%, so that 87% of the positrons were initially channeled. This remarkable result demonstrates that, under optimal conditions, it is possible to channel nearly *all* of the positrons.

D. 16.9-MeV electron data

16.92-MeV electron (100) and (110) spectra from a 7.8-μm-thick silicon crystal are displayed in Figs. 14 and 15. As for the 54.5-MeV electron and positron data, the absolute flux of the CR was determined by comparison with the calculated bremsstrahlung flux (corrected for multiple scattering and absorption). Since there are only two bound states in the (100) potential well for 16.92-MeV electrons, there is only one CR peak in the spectrum. This makes it easy to determine the absolute flux of the $1\rightarrow0$ peak, which is displayed in Fig. 16, along with integrated-exponential and multiple-scattering fits.

The $1/e$ occupation length of the $n=1$ level is about 16 μm, somewhat less than the 24-μm length measured or 54.5-MeV electrons for the same plane. The slope of the curve at the origin is about 0.0031 photons/(e^- sr μm), as compared with a calculated flux (which assumes 100% population in the $n=1$ level) of 0.027 photons/(e^- sr μm), which implies that the initial population of the $n=1$ level is about 12%.

The 16.92-MeV electron (110) spectrum is particularly interesting because it exhibits several well-separated peaks, providing an opportunity to study the evolution of the population of several different bound states individually. The $3\rightarrow2$ and $3\rightarrow0$ peaks both contain information about the $n=3$ level. However, the $3\rightarrow2$ peak is at such a low photon energy (only 6 keV) that the detector efficiency is extremely small (so that even a small amount of noise can distort or obscure it). Furthermore, the $3\rightarrow2$ peak is absorbed very strongly in the thicker silicon crystals. Consequently, the $3\rightarrow0$ peak (which is at 35 keV) is a better measure of the population despite its

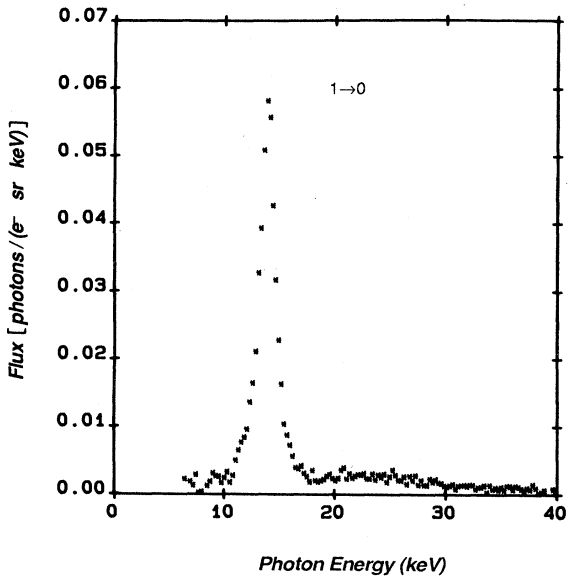

FIG. 14. Observed CR spectrum from 16.9-MeV electrons channeled by the (100) plane of a 19-μm-thick silicon crystal.

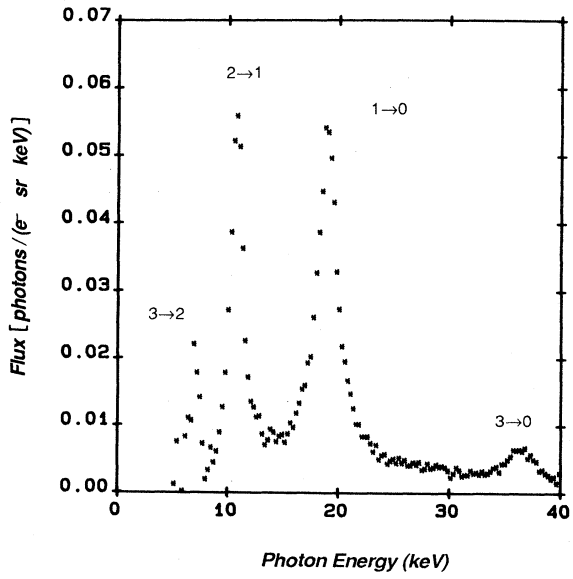

FIG. 15. Observed CR spectrum from 16.9-MeV electrons channeled by the (110) plane of a 19-μm-thick silicon crystal.

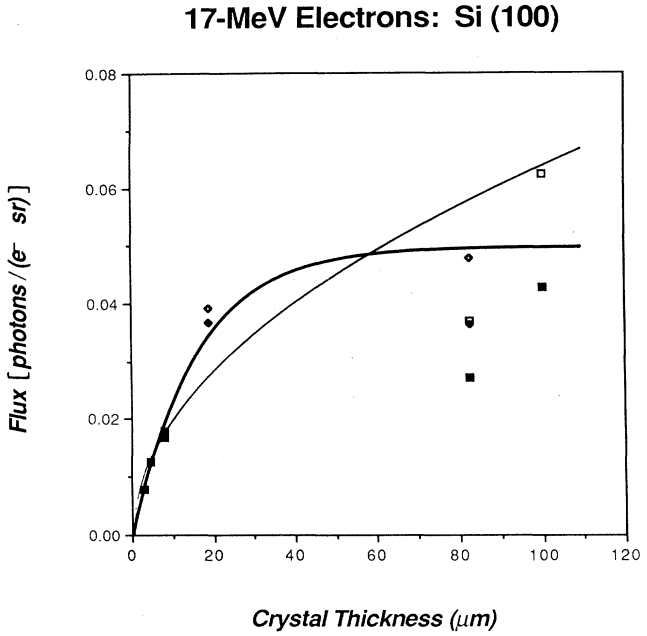

FIG. 16. Measured CR flux in the $1\rightarrow0$ peak for 16.9-MeV electrons channeled by the (100) plane of silicon as a function of crystal thickness. The different symbols represent different experimental conditions. For thicknesses greater than 10 μm, the absorption-corrected fluxes are represented by open squares. the "multiple-scattering" fit, $0.0064Z\ (\mu\text{m})^{1/2}$, is represented by the thin solid curve; the "integrated-exponential" fit, $0.05\ (1-e^{-Z(\mu\text{m})/16})$, is represented by the thick solid curve.

lesser intensity. The measured fluxes of the $1\rightarrow0$, $2\rightarrow1$, $3\rightarrow2$, and $3\rightarrow0$ transitions have been multiplied by the absorption correction factor $\exp[\mu(E_\gamma)Z]$ of Eq. (6) and plotted as a function of thickness in Figs. 17(a)–17(d). From the $1\rightarrow0$, $2\rightarrow1$, and $3\rightarrow0$ transitions, the $1/e$ occupation lengths for the $n=1$, $n=2$, and $n=3$ levels are found to be 20, 20, and 17 μm, respectively. There is one further adjustment to make in the $2\rightarrow1$ data. Since the peak is situated at about 10 keV, the x-ray absorption length is not that much greater than the occupation length (120 μm versus about 20 μm), so in this case the exponential factor inside the integral in Eq. (6) cannot be ignored. Assuming that the decay in population is exponential, the true occupation length must be given by a parallel sum of 120 and 20 μm, or 17 μm. These $1/e$ lengths are equal to within the experimental uncertainty, which means that the bound-state populations maintain the same relative proportions throughout the thickness of the crystal (as was true for 54-MeV electrons and positrons).

The slopes of the integrated-exponential fits in Figs. 17(a), 17(b), and 17(d) are 0.0029, 0.0019, and 0.000 27 photons/(e^- sr μm), as compared with calculated fluxes of 0.053, 0.033, and 0.0043 photons/(e^- sr μm), giving measured initial populations of 5.5% for $n=1$, 5.6% for $n=2$, and 6.3% for $n=3$.

The measured value of 12% for the (100) plane is consistent with a beam divergence of 1.8 mrad. If one assumes the same beam divergence for the (110) plane, the calculated initial populations are 7.7% for the $n=1$, $n=2$, and $n=3$ levels. This is somewhat higher than the measured populations of about 6%. The (110) initial populations are more consistent with a beam divergence of about 2.5 mrad. It is not inconceivable that the beam divergence may have been different for the two planes, since the beam was noticeably elliptical when viewed on a fluorescent screen located near the Ge detector.

E. The effect of multiple scattering on CR peaks

Having obtained an approximate form for the populations $p_n(z)$, it is possible (in principle) to insert this into Eq. (5) in order to elucidate the multiple-scattering distribution for channeled particles $f_n(\theta,z)$. As discussed in Sec. III, it is natural to assume that $f_n(\theta,z)$ has the form of a Gaussian with a multiple-scattering angle proportional to $z^{1/2}$. The 17-MeV electron (100) and (110) $1\rightarrow0$ peaks are sufficiently distinct from other peaks that one might hope to determine the proportionality constant by measuring the asymmetric distortion of the peak resulting from the Doppler shift. However, a close analysis of the line shapes reveals little perceptible broadening or asymmetry. Evidently, multiple scattering of channeled 17-MeV electrons within the first 15 μm is negligible. One would expect to see some distortion of the $1\rightarrow0$ peaks if the multiple-scattering angle were as large as half of $1/\gamma$ (or about 15 mrad) after 15 μm. This establishes that $A(z=15\ \mu\text{m})^{1/2}<15$ mrad, where A is the proportionality constant mentioned above. This upper bound of $A<4$ can be compared with the corresponding proportionality constant for unchanneled particles: $\Theta(z)$ (mrad)$=2.5[z(\mu\text{m})]^{1/2}$, where Θ is the projection of the multiple-scattering angle of randomly directed particles in one dimension.

Thus, multiple scattering of channeled 17-MeV electrons in silicon is less than twice that of unchanneled particles. This is consistent with the fact that the bremsstrahlung yield from channeled particles is only slightly greater than that from unchanneled particles. In the case of 17-MeV electrons in silicon, multiple scattering does not contribute appreciably to the CR linewidth, nor does it shift the centroids by a perceptible amount.

For 54-MeV positrons, the observed spectra of Fig. 6 fail to exhibit the sharp spikes of the calculated spectrum in Fig. 6(a). The widths of these spikes are comparable to or slightly greater than the resolution of the detector in this spectral region, so the spikes ought to be observable if they are present. The failure to observe these spikes may be attributable to multiple scattering, which is not included in the calculation displayed in Fig. 6(a). As shown in Fig. 18, the fine structure of the composite peak is almost washed out when normal multiple scattering is included in the calculation. Since positrons tend to avoid the dense electron clouds which surround atomic nuclei, one would expect the multiple scattering of channeled positrons to be somewhat less than that of randomly-directed positrons. Apparently, if multiple scattering is the primary source of line broadening for channeled posi-

trons (aside from anharmonic broadening), its magnitude is not *very* much less than that of randomly-directed positrons. One cannot exclude the possibility that plasmons, which are present in the region between the planes (where the positrons channel) may induce some scattering which could help to wash out the spectrum (and even shift the spectral peak downward).[30]

VI. DISCUSSION OF RESULTS AND CONCLUSION

The $1/e$ occupation lengths are summarized in Table I. Several trends are evident. The occupation length of channeled electrons increases slowly with beam energy—in the neighborhood of 50% to 100% when the beam energy is tripled from 17 to 54 MeV. These results conflict with the results of Komaki *et al.*,[14] who obtained a $1/e$ length of only 31 μm for 350-MeV electrons channeled by Si(110) planes. The occupation length is longer for the (110) plane than for the (100) plane for all of the cases studied. This may be attributable to the

TABLE I. Measured $1/e$ lengths (in μm) for 17- and 54-MeV electrons and 54-MeV positrons channeled by the major planes of silicon. The uncertainties in these figures are estimated to be approximately $\pm 20\%$.

	(100)	(110)	(111)
17-MeV e^-	16	20 ($n=1$)	
		17 ($n=2$)	
		17 ($n=3$)	
54-MeV e^-	24	36	
54-MeV e^+	40	60	42

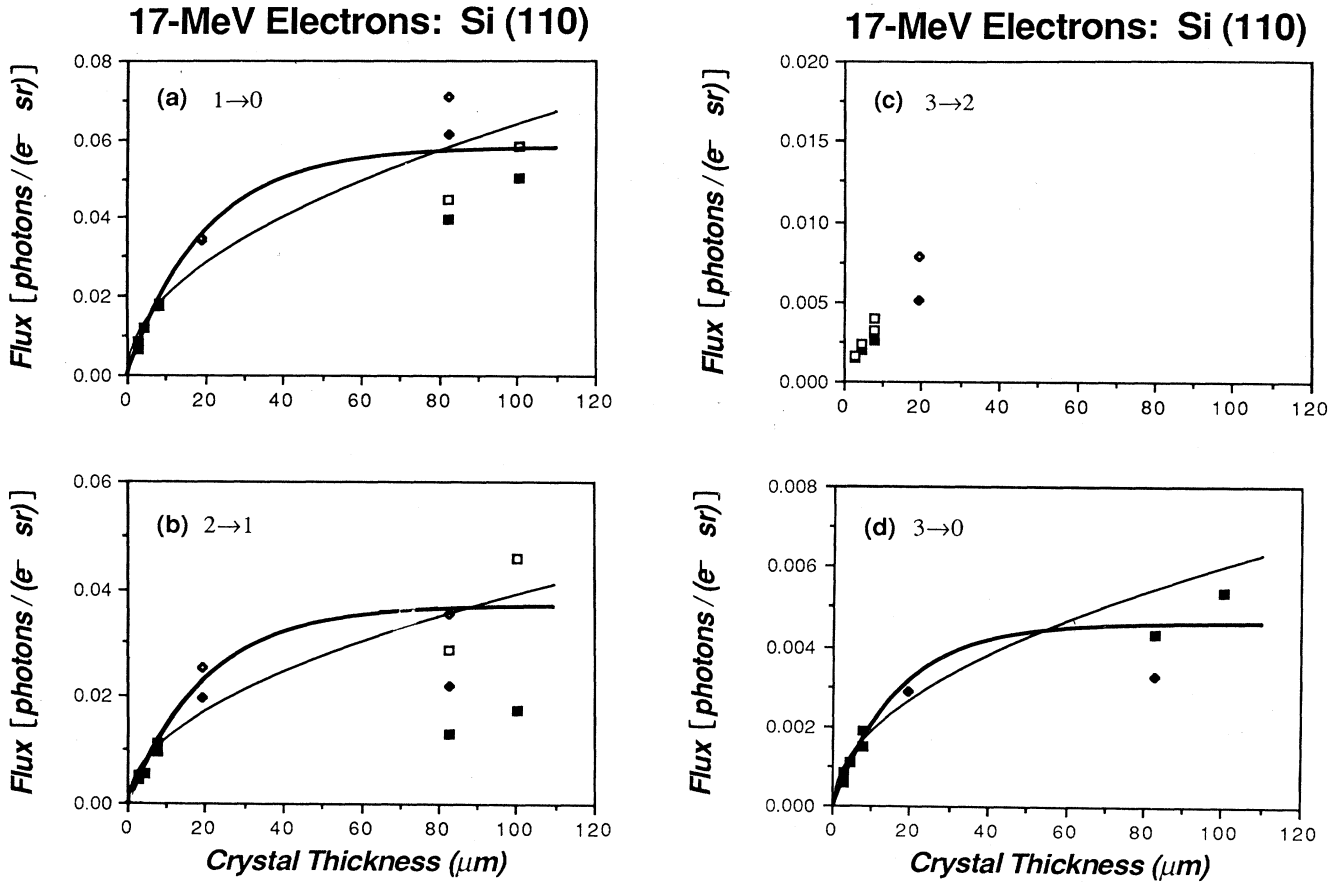

FIG. 17. Measured flux of the four peaks in the CR spectrum of 16.9-MeV electrons channeled by the (110) plane of silicon as a function of crystal thickness. The different symbols represent different experimental conditions. For thicknesses greater than 10 μm, the absorption-corrected fluxes are represented by open squares. The "multiple-scattering" fits are represented by thin solid curves; the "integrated-exponential" fits are represented by thick solid curves. (a) $1\rightarrow 0$ peak. The "multiple-scattering" and "integrated exponential" fits are $0.0064Z\ (\mu\text{m})^{1/2}$ and $0.058(1-e^{-Z(\mu\text{m})/20})$, respectively. (b) $2\rightarrow 1$ peak. The "multiple-scattering" and "integrated exponential" fits are $0.0039Z\ (\mu\text{m})^{1/2}$ and $0.037(1-e^{-Z(\mu\text{m})/20})$, respectively. (c) $3\rightarrow 2$ peak. (d) $3\rightarrow 0$ peak. The "multiple-scattering" and "integrated exponential" fits are $0.0006Z\ (\mu\text{m})^{1/2}$ and $0.046(1-e^{-Z(\mu\text{m})/17})$, respectively.

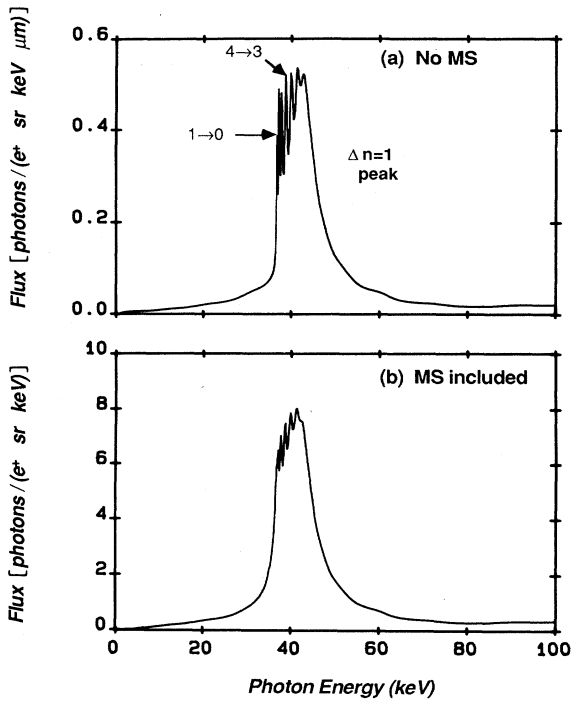

FIG. 18. The effect of normal multiple scattering on the calculated CR spectrum of 54-MeV positrons channeled by the (110) plane for silicon (a) without multiple scattering and (b) with multiple scattering.

greater depth of the (110) potential well. On the average, particles trapped in a (110) potential have to acquire more transverse energy in order to become dechanneled than do particles trapped in a (100) potential.

It is somewhat surprising that the 54-MeV positron occupation lengths are not *very* much greater than the 54-MeV electron occupation lengths. One would expect them to be quite a bit longer because the positrons tend to avoid the vibrating atomic nuclei. This might indicate that something else (possibly atomic electrons, plasmons, impurities, or defects) scatters the positrons. Despite the fact that 54-MeV positron occupation lengths in silicon are only of the order of 50 μm, the amount of forward-directed CR generated in the $\Delta n = 1$ peak within those 50 μm is substantially greater than the amount of forward-directed bremsstrahlung produced in the same spectral region through a thickness of several mm.

The measured initial populations are summarized in Table II. For these experiments, the electron beam divergence was large enough so that the initial bound-state populations were essentially equal to one another. By comparing the shapes of processed CR spectra observed from crystals with a range of thicknesses (as in Figs. 5 and 6), it has been established that, for 54-MeV electrons, the relative populations of the bound states do not change appreciably. This has been verified for the (110) and (111) planes as well as for the (100) plane. In the case of the 17-MeV (110) data, the spectral peaks are sufficiently distinct to allow separate determination of the occupation lengths for the $n = 1$, 2, and 3 levels—20, 17, and 17 μm, respectively. In other words, the bound-state populations remain nearly equal relative to one another for 17-MeV electrons as well as for 54-MeV electrons.

For positrons, the beam divergence also was large enough to populate the bound states equally. Individual transitions are not resolvable in the $\Delta n = 1$ peak, but the linewidth and line shape of the peak in the 19- and 100-μm data for all three planes are consistent with the calculated spectra, in which equal populations are assumed. Therefore, it can be concluded that whenever the bound-state populations are initially equal, they will remain approximately equal to one another throughout the thickness of the crystal.

Another conclusion which can be drawn from the similarity of the shapes of the CR spectra observed from crystals with different thicknesses is that multiple scattering has little influence upon the CR spectra. Apparently, the occupation length is short enough so that little multiple scatering can occur before the particle is dechanneled. Contrary to what one might expect, the multiple scattering of channeled electrons is not significantly greater than that of randomly-directed electrons. This is consistent with our observation that channeled electrons do not produce much more bremsstrahlung than randomly-directed electrons (Sec. IV). These observations support the conclusion of Gouanère *et al.*[19] that the many-beam theory predicts *coherent* processes such as channeling radiation and coherent bremsstrahlung spectra very well but overestimates a variety of *incoherent* processes such as bremsstrahlung and multiple scattering.

Unfortunately, the asymptotic form of the population decay of channeled particles [i.e., exponential decay or

TABLE II. Measured initial populations of 17- and 54-MeV electrons and 54-MeV positrons channeled by the major planes of silicon compared with theoretical initial populations based upon beam divergence.

		Avg. beam divergence (mrad)	(100) Meas.	(100) (Theor.)	(110) Meas.	(110) (Theor.)	(111) Meas.	(111) (Theor.)
			(%)		(%)		(%)	
17-MeV e^-	($n=1$)	2.2	11.6	(9.2)	5.5	(6.5)		
	($n=2$)				5.6	(6.5)		
	($n=3$)				6.3	(6.5)		
54-MeV e^-		1.0	6–7	(8.2)	4–5	(4.3)		
54-MeV e^+		1.2	5.3	(5.5)	2.8	(3.7)	2.5	(2.4)

multiple scattering ($Z^{-1/2}$)] cannot be extracted from the data because of the scatter. This scatter could be reduced substantially in future experiments by increasing the beam current by at least two orders of magnitude so that it could be measured reliably, obviating the need for thick-target bremsstrahlung normalization (the validity of which is questionable for extremely thick crystals). Increasing the beam current would make single-photon counting impossible and therefore necessitate a different x-ray detection system. In addition, it would be important to measure the beam divergence directly (rather than having to infer it from the CR spectra).

It would be quite interesting to use beams with lower divergences in order to observe the equilibration of bound-state populations with one another. From Fig. 10, it is apparent that such a regime would be reached with a beam divergence of about 0.2 to 0.5 mrad. A wide variety of initial population distributions could be achieved by intentionally misaligning the crystal by a few tenths of a mrad. Equilibration then would occur on a shorter length scale than the occupation lengths that have been measured in the experiments reported here. In such a case, the concept of an occupation length would be an almost useless oversimplification—the evolution of the populations would be governed by coupled rate equations and would therefore depend critically upon the initial distribution.

ACKNOWLEDGMENTS

The authors thank Nancy del Grande of the Lawrence Livermore National Laboratory for measuring the thickness of several of the thinner silicon crystals. This work was supported by the U.S. Air Force Office of Scientific Research under Grant No. F49620-86-K-0015.

[1]J. Lindhard, K. Dan. Vidensk. Selsk. Mat. Fys. Medd. **34**, 14 (1965).

[2]D. S. Gemmel, Rev. Mod. Phys. **46**, 129 (1974).

[3]A. F. Elishev, N. A. Filatova, V. M. Golovatyuk, I. M. Ivanchenko, R. B. Kadyrov, N. N. Karpenko, V. V. Korenkov, T. S. Nigmanov, V. D. Riabtsov, M. D. Shafranov, B. Sitar, A. E. Senner, B. M. Starchenko, V. A. Sutulin, I. A. Tyapkin, E. N. Tsyganov, D. V. Uralsky, A. S. Vodopianov, A. Forycki, Z. Guzik, J. Wojtkowska, R. Zelazny, I. A. Grishaev, G. D. Kovalenko, B. I. Shramenko, M. D. Bavizhev, N. K. Bulgakov, V. V. Avdeichikov, R. A. Carrigan Jr., T. E. Toohig, W. M. Gibson, Ick-Joh Kim, J. Phelps, and C. R. Sun, Phys. Lett. **88B**, 387 (1979).

[4]J. F. Bak, P. R. Jensen, H. Madsbøll, S. P. Møller, H. E. Schiøtt, E. Uggerhøj, J. J. Grob, and P. Siffert, Nucl. Phys. **B242**, 1 (1984).

[5]J. U. Andersen, E. Bonderup, and R. H. Pantell, Annu. Rev. Nucl. Part. Sci. **33**, 453 (1983).

[6]R. K. Klein, J. O. Kephart, R. H. Pantell, H. Park, B. L. Berman, R. L. Swent, S. Datz, and R. W. Fearick, Phys. Rev. B **31**, 68 (1985).

[7]V. V. Beloshitskii and M. A. Kumakhov, Zh. Eksp. Teor. Fiz. **74**, 1244 (1978) [Sov. Phys.—JETP **47**, 652 (1978)].

[8]Y. H. Ohtsuki, Nucl. Instrum. Methods B **2**, 80 (1984).

[9]A. V. Andreev, S. A. Akhmanov, and V. L. Kuznetsov, Pis'ma Zh. Tekh. Fiz. **7**, 682 (1981) [Sov. Tech. Phys. Lett. **7**, 292 (1981)].

[10]G. Kurizki, in *Relativistic Channeling,* edited by Richard A. Carrigan, Jr. and James A. Ellison (Plenum, New York, 1987).

[11]V. I. Vysotskii and R. N. Kuz'min, Pis'ma Zh. Tekh. Fiz. **53**, 1254 (1983) [Sov. Phys. Tech. Phys. **28**, 768 (1983)].

[12]J. U. Andersen, E. Bonderup, E. Laegsgård, B. B. Marsh, and A. H. Sørensen, Nucl. Instrum. Methods **194**, 209 (1982).

[13]W. Beezhold, T. W. L. Sanford, H. Park, J. O. Kephart, R. K. Klein, R. H. Pantell, B. L. Berman, and S. Datz, Bull. Am. Phys. Soc. **30**, 374 (1985); and (unpublished).

[14]K. Komaki, A. Ootuka, F. Fujimoto, N. Horikawa, T. Nakanishi, C. Y. Gao, T. Iwata, S. Fukui, M. Mutou, and H. Okuno, Nucl. Instrum. Methods B **2**, 71 (1984).

[15]V. V. Beloshitskii and M. A. Kumakhov, Zh. Eksp. Teor. Fiz. **82**, 462 (1982) [Sov. Phys.—JETP **55**, 265 (1982)].

[16]V. A. Muralev, Phys. Status Solidi B **118**, 363 (1983).

[17]J. U. Andersen, K. R. Eriksen, and E. Laegsgård, Phys. Scr. **24**, 588 (1981).

[18]B. L. Berman and S. Datz, in *Coherent Radiation Sources,* edited by A. W. Saenz and H. Uberall (Springer-Verlag, Berlin, 1985).

[19]M. Gouanère, D. Sillou, M. Spighel, N. Cue, M. J. Gaillard, R. G. Kirsch, J-C. Poizat, J. Remillieux, B. L. Berman, P. Catillon, L. Roussel, and G. M. Temmer, Phys. Rev. B **38**, 4352 (1988).

[20]G. Radi, Acta Crystallogr. Sect. A **26**, 41 (1970).

[21]W. T. Scott, Rev. Mod. Phys. **35**, 256 (1963).

[22]V. L. Highland, Nucl. Instrum. Methods **129**, 497 (1975).

[23]E. V. Hungerford and B. W. Mayes, At. Data Nucl. Data Tables **15**, 477 (1975).

[24]J. D. Jackson, *Classical Electrodynamics,* 2nd ed. (Wiley, New York, 1975).

[25]J. O. Kephart, Ph.D. thesis, Standford University, 1988, pp. 283–308.

[26]R. C. Weast, *CRC Handbook of Physics and Chemistry,* 57th ed. (CRC, Cleveland, 1976).

[27]EG&G Ortec Radiation Detection Catalog, 1984, p. 64.

[28]E. F. Plechaty, D. E. Cullen, and R. J. Howerton, Lawrence Livermore National Laboratory Report No. UCRL-50400, Vol. 6, Rev. 3, 1981 (unpublished).

[29]H. W. Koch and J. W. Motz, Rev. Mod. Phys. **31**, 920 (1959).

[30]P. Amendt, M. Strauss, H. U. Rahman, and N. Rostoker, Phys. Rev. A **33**, 839 (1986).